Temperature-dependent structure-activity relationship of OH + haloalkene rate coefficients under atmospheric conditions and supporting measurements

Lisa Michelat, Abdelwahid Mellouki, A R Ravishankara, Hajar El Othmani, Vassileios C Papadimitriou, Véronique Daële, Max R Mcgillen

Temperature-dependent structure-activity relationship of OH + haloalkene rate coefficients under atmospheric conditions and supporting measurements

Journal:	*ACS Earth and Space Chemistry*
Manuscript ID	sp-2022-00296a.R2
Manuscript Type:	Article
Date Submitted by the Author:	n/a
Complete List of Authors:	Michelat, Lisa; Institut de Combustion Aérothermique Réactivité et Environnement Mellouki, Abdelwahid; CNRS, ICARE/OSUC Ravishankara, Akkihebbal; Colorado State University, Departments of Chemistry and Atmospheric Science; Le Studium Institute for Advanced Studies El Othmani, Hajar; Institut de Combustion Aérothermique Réactivité et Environnement Papadimitriou, Vassileios; University of Crete Department of Chemistry, Chemistry Daële, Véronique; Institut de Combustion Aérothermique Réactivité et Environnement McGillen, Max; Institut de Combustion Aérothermique Réactivité et Environnement,

Temperature-dependent structure-activity relationship of OH + haloalkene rate coefficients under atmospheric conditions and supporting measurements

Lisa Michelat[1], Abdelwahid Mellouki[1], A.R. Ravishankara[2,3], Hajar El Othmani[1], Vassileios C. Papadimitriou[4], Véronique Daële[1], and Max R. McGillen[1]*

[1] Institut de Combustion, Aérothermique, Réactivité et Environnement (ICARE), CNRS/OSUC, 45071 Orléans, Cedex 2, France

[2] Departments of Chemistry and Atmospheric Science, Colorado State University, Fort Collins, CO 80523, USA

[3] Le Studium of the Loire Valley, 45000, Orléans, France

[4] Laboratory of Photochemistry and Chemical Kinetics, Department of Chemistry, University of Crete, 70013 Heraklion, Crete, Greece

Keywords: Hydrofluoroolefin, rate constant, atmospheric chemistry, Arrhenius parameters, structure-activity relationship

Abstract:

Hydrofluoroolefins (HFOs) and related haloalkenes are a family of compounds, primarily man-made, with many industrial applications. Gas-phase electrophilic addition of OH to the olefinic bond represents the primary sink for these chemicals in the atmosphere. The degree and type of halogenation strongly affect their chemical reactivity, leading to differing reactivities with the OH radical that have presented a challenge for structure-activity relationships (SARs). Here, we investigate and extend the SARs to estimate temperature-dependent OH reaction rate coefficients, $k(T)$, at tropospheric temperatures.

We considered two techniques: the group-additivity approach of Atkinson and co-workers and the recent method of Tokuhashi and co-workers; we found the latter to make superior predictions for halogenated olefins. We extended Tokuhashi *et al.*'s SAR to include more olefins and to predict temperature dependencies.

We compared SAR predictions against new absolute $k(T)$ for two HFOs (3,3,3-trifluoropropene and 1,1,3,3-tetrafluoropropene) measured using the pulsed-laser photolysis–laser-induced fluorescence technique from 212 to 373K. The Arrhenius expressions were determined as $k_{OH+CF3CH=CH2}(T) = (8.86\pm0.82)\times10^{-13}\exp[(159\pm26)/T]$ and $k_{OH+CF2HCH=CF2}(T) = (7.46\pm0.34)\times10^{-13}\exp[(365\pm12)/T]$. The measured $k(T)$ was predicted accurately between 200 and 400K using the modified Tokuhashi approach. Our new measurements of the OH reaction rate coefficient with 3,3,3-trifluoropropene were in excellent agreement with literature determinations. We represent the first reported $k(T)$ for 1,1,3,3-tetrafluoropropene.

Given that new HFOs enter the market frequently, such estimation techniques may be a helpful screening tool for assessing their environmental impact before they are examined further and reach the mass–production phase.

1. Introduction:

Following the Montreal Protocol and its amendments, ozone-depleting substances continue to be replaced by new generations of substitutes, which are less harmful to the climate and the ozone layer.[1,2] In particular, the recent Kigali amendment is phasing out high global warming potential (GWP)

hydrofluorocarbons (HFCs).[2] Hydrofluoroolefins (HFOs), which are very short-lived fluorinated gases with low GWPs, are substitutes that are increasing in use.[3]

HFOs have found many industrial applications as refrigerants, propellants, and foam-blowing agents. Composed of fluorine, hydrogen, and an olefinic carbon backbone, they represent a subset of the broader class of haloalkenes, which contain any combination of olefin and halogen substitution. Such olefins have many additional uses as solvents, cleaning fluids, and feedstocks for polymers. Due to their widespread usage, HFO emissions are increasing in the atmosphere, and atmospheric monitoring programs are now detecting them.[4] HFOs and related haloalkenes are primarily removed from the troposphere via electrophilic addition of the OH radical to the double bonds within them. Accurate knowledge of the OH reaction rate coefficient is valuable because it can be incorporated into atmospheric models that assess their contribution to air pollution, stratospheric ozone depletion, and global warming.[1]

A large variety of haloalkenes are already in use and the global demand for efficient but environmentally friendly cooling technologies is growing.[5] It is likely that many new haloalkenes proposed as replacements have yet to have their OH reaction rate coefficients measured. For initial consideration of uses, it is therefore desirable to have reliable estimates of these rate coefficients; which is the main focus of the present work.

Structure-activity relationships (SARs) have been used extensively to estimate reaction rate coefficients by correlating the chemical structure of a species with its reactivity.[6] From trends in available kinetic data, SARs derive satisfactory predictions applicable to a broader set of chemicals for which rate coefficients are unavailable. Similarly, the development and improvement of SARs are becoming increasingly necessary as atmospheric chemical models become more explicit and complete.[6] Furthermore, in the process of parameterizing the chemical reactivity that SAR-development entails, we aim to improve the chemical understanding of the mechanism of the electrophilic addition of OH radicals to alkenes.

We estimated room-temperature OH reaction rate coefficients of haloalkenes, k_{298}, from the AOPWIN v1.92 module of the estimation programs interface EPI Suite[7,8] based on the approach of Kwok and Atkinson.[9] We also applied the more recent method of Tokuhashi *et al.*[13-17] to calculate k_{298} and extended it to predict temperature-dependent rate coefficients, $k(T)$, between 200 and 400 K. We assume that the addition reactions are at their high-pressure limit and thus the pressure is not a parameter that influences the rate coefficients. We compared these calculations with new laboratory measurements of the absolute OH reaction rate coefficients as a function of the temperature of two HFOs, $CF_3CH{=}CH_2$ (212–367 K) and $CF_2HCH{=}CF_2$ (223–373 K), using the pulsed-laser photolysis–laser-induced fluorescence (PLP–

LIF) technique. The reaction of $CF_3CH=CH_2$ with OH has been studied previously at various temperatures,[18-23] whereas the rate coefficient of $CF_2HCH=CF_2$ with OH has never been reported to the best of our knowledge.

2. Methodology:

2.1. Structure-activity relationships (SARs) :

2.1.1. Literature methods:

In this section, we outline the existing methods to predict k_{298} from the structure of an olefin. We note that Tokuhashi's method[13-17] and the implementation of Atkinson's SAR[9-12] by AOPWIN[7-8] are both limited to room temperature (298 K).

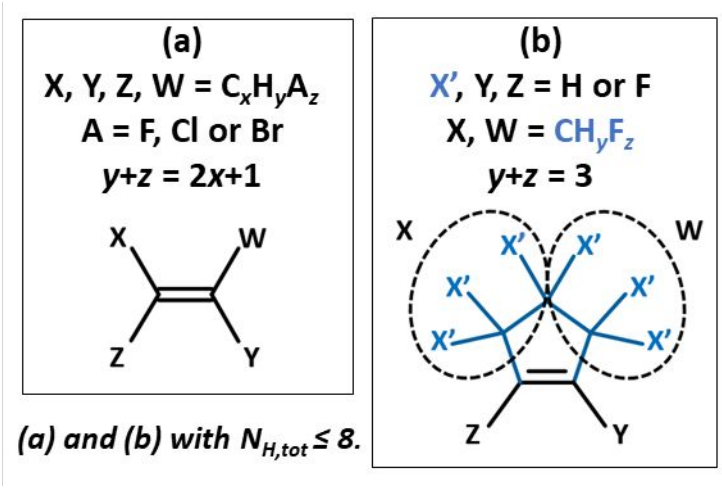

Figure 1: Schematic of the structure of the alkenes used in the models, with (a) being the description applied for acyclic alkenes where X, Y, Z, W substituents are defined by $C_xH_yA_z$ where A = F, Cl or Br and where $y + z = 2x+1$, where $x \geq 0$ and (b) referring specifically to the cyclic olefins containing H and F substitutions only, both (a) and (b) defined for molecules with a total hydrogen count, $N_{H,tot}$, of ≤8. In structure (b), X', Z, and Y substituents can be either H or F atoms. The two groupings X and W are defined by splitting the cycle into two symmetrical chains, each possessing three X' atoms in the case of a cyclopentyl group. In Tokuhashi *et al.*'s recent work,[17] only linear olefins, as in structure (a), are described, excluding Br substitutions and limited to values of $x \leq 2$.

2.1.1.1. Atkinson approach

The AOPWIN v1.92 program output for olefins includes estimations of the gas-phase hydroxyl radical

reaction rate coefficients at 298 K.[7-8] These estimations are built upon the work of Atkinson and co-workers, with the most recent update described in Kwok and Atkinson's paper.[9] This method estimates the reactivity of a large number of alkenes, which themselves are part of a broader approach that also predicts the reactivity of saturated organic molecules. For halogenated alkenes, the overall calculated OH reaction rate coefficient is dominated by the reactivity of the C=C bond towards OH radical electrophilic addition with generally negligible contributions from the H-abstraction channel. Depending on the identity of the substituents, the reactivity of the alkene is expected to be affected by the electron-withdrawing inductive effects, the electronegativity of the halogenated group(s), the possible interplay between these groups and their respective positions. For a halogenated alkene of formula X(Z)C=C(W)Y (see Structure (a) in Figure 1), the room temperature rate coefficient towards the OH reaction is calculated as follows:

$$k_{298,\mathrm{Atkinson}}\mathrm{X(Z)C{=}C(W)Y} = k_{\mathrm{base}} \times F(\mathrm{X}) \times F(\mathrm{Y}) \times F(\mathrm{Z}) \times F(\mathrm{W}) \quad (1)$$

where k_{base} is the base rate coefficient of the associated generic alkene, -C=C, -C=C-, >C=C, >C=C- or >C=C<, and its stereoisomer (*cis* or *trans*), and F(X), F(Y), F(Z), F(W) are multiplicative constants that are specific to a functional group (X, Y, Z, W being halogens or alkyl groups).[9] For further details on the method, readers are directed to the original papers from Atkinson[10-12] and Kwok and Atkinson,[9] or the website of the EPI Suite interface that implements AOPWIN.[7,8]

For halogenated alkyl groups, i.e., allylic halogen substitutions, a constant value for "F(–Halogen)" of 0.76 is employed in Atkinson approach to describe the substitution effect.[9] If halogen substitutions of the alkenes are more distant than the allyl position with respect to the olefinic bond, these compounds are treated as regular alkenes. Consequently, such an implementation becomes degenerate towards many possible permutations on the alkyl group.

2.1.1.2. Tokuhashi's method - Diagonal substituent factors:

A method for estimating OH reaction rate coefficients of halogenated alkenes was more recently developed by Tokuhashi and co-workers (see [13-17]). In that work, the authors consider that a haloalkene's reactivity is related to the identity of the substitution and the position of these substituents around the double bond. The diagonal substitution pattern across the olefinic bond was found to be a critical parameter that alters the rate coefficient.

In their previous work on halogenated ethenes,[15] Tokuhashi and co-workers observed that the experimentally determined rate coefficients for these compounds are determined not only by the type of substituents attached to the double bond but also on the substituent on the opposite side of the olefinic

bond. By considering this substitution position, Tokuhashi *et al.*[13-17] have developed a method that can reproduce the available experimental data within a factor of two, with a few exceptions.

Substituent factors are designed to account for the changes in the electron density in the π-orbitals, which are expected to be of primary importance in describing the reactivity of the double bond towards an electrophilic addition of OH. The calculated OH rate coefficient at room temperature is obtained by:

$$k_{298,\text{Tokuhashi}}\text{X(Z)C=C(W)Y} = k_{\text{base}} \times F(\text{X-C=C-Y}) \times F(\text{Z-C=C-W}) \quad (2)$$

The base rate coefficient, $k_{\text{base}} = 1.0 \times 10^{-12}$ cm^3 molecule^{-1} s^{-1},[13,17] is that of the unsubstituted case. The terms F(X-C=C-Y) and F(Z-C=C-W) are the substituent factors for the structures shown in parentheses. The X-C=C-Y and Z-C=C-W represent diagonal positions (see Structure (a), Figure 1), as defined by Tokuhashi *et al.*[13-17]

2.1.2. This work (modified Tokuhashi approach)

In this section, our approach will be described as an updated and extended version of the Tokuhashi method described in section 2.1.1.2.[13] In the original work of Kwok and Atkinson[9] and that of Tokuhashi *et al.,*[13,17] the rate coefficient for OH-addition to cycloalkenes is not estimated. In the AOPWIN program, in contrast, k_{298} are predicted for the presence of a ring by treating them as linear alkenes with a structure separated into two symmetrical chains on both sides of the double bond. Based on Equation 2, the OH-reaction rate coefficient of $CF_3CF=CFCF_3$ (structure #54, see Figure 2) would be identical to that of the cyclic perfluorocyclopentene (#63). However, the acyclic compound in this case has a much larger rate coefficient than the cyclic compound. Hence, the difference in reactivities may be a consequence of the ring strain, and/or the supplementary steric effects encountered in cyclic structures compared to linear geometries.[24] Our approach is speculative given the sparsity of experimental data for cyclic halogenated olefins, and we use a single additional factor F_{cycle} to account for the difference in reactivity. As new data become available, this factor may be expanded as a function of ring size.

Hence, the model built in the present work estimates k_{298} for the electrophilic addition reaction of OH with molecule X(Z)C=C(W)Y from the following formula:

$$k_{298,\text{calc}} = k_{\text{base}} \times F(\text{X-C=C-Y}) \times F(\text{Z-C=C-W}) \times F_{\text{cycle}} \quad (3)$$

where $k_{\text{base}} = 1.0 \times 10^{-12}$ cm^3 molecule^{-1} s^{-1}, which is intended to represent the base-level reaction rate coefficient of electrophilic addition to the >C=C< bond. The F-factors in Equation 3 include the substituent factors, F(X-C=C-Y) and F(Z-C=C-W) that account for the diagonal structure around the olefinic bond (see structures (a) and (b), Figure 1), and F_{cycle} that accounts for an olefin's cyclic structure.

If alkenes are acyclic, F_{cycle} is 1. Because of the need to distinctly define each diagonal substitution across the double bond in this method, we excluded rate coefficients reported for undefined stereoisomers or a mixture of *E* and *Z* isomers from the training set.

The calculated k_{298} values were optimized using a numerical solver that optimized the *F*-factor values in order to minimize the relative difference between estimated and experimental results, defined as $RE(\%)=100\times(k_{298,calc}-k_{298,meas})/k_{298,meas}$. The resulting optimized *F*-factors are presented in section 3.2. Additionally, our SAR provides a method to estimate the temperature-dependent reaction rate coefficient, $k(T)$, based on the values of the calculated k_{298}, and the Arrhenius equation, as presented in section 3.4.

2.2. Rate coefficient measurements of the reaction of OH with $CF_3CH=CH_2$ and $CF_2HCH=CF_2$:

2.2.1. Apparatus Description:

The rate coefficients for OH reaction with two HFOs, $CF_3CH=CH_2$ and $CF_2HCH=CF_2$, were measured between 212 and 367 K, and 223 and 373 K, respectively, using a pulsed-laser photolysis–laser-induced fluorescence (PLP–LIF) apparatus (Figure 2) described elsewhere.[25,26]

The OH radicals were produced by photolysis of hydrogen peroxide (H_2O_2) or nitric acid (HNO_3) using a pulsed KrF excimer laser (PLP) (λ = 248 nm, 25–85 mJ pulse^{-1} cm^{-2} in the reaction cell) inside a 200 cm^3 Pyrex reactor:

$$H_2O_2 + h\nu \rightarrow 2OH \qquad (7)$$

$$HNO_3 + h\nu \rightarrow OH + NO_2 \qquad (8)$$

The initial hydroxyl radical concentrations, $[OH]_0$, were varied in the ranges (1.7–30.6) × 10^{10} molecule cm^{-3} for the reaction with $CF_3CH=CH_2$ and (6.7–279.0) × 10^{10} molecule cm^{-3} for the reaction with $CF_2HCH=CF_2$ (see Equation S1). The output of an Nd:YAG pumped dye laser (Rhodamine 590) was doubled and used to excite the Q_11 line in the (1,0) band of the ($A^2\Sigma^+$,*v*'=1) ← ($X^2\Pi$,*v*"=0) transition of OH radicals near 282 nm. The resulting OH fluorescence signals emitted from the ($A^2\Sigma^+$, *v*'=1) → ($X^2\Pi$, *v*"=1) and ($A^2\Sigma^+$, *v*'=0) → ($X_2\Pi$, v'=0) transitions (308–316 nm) were detected by a photomultiplier tube (equipped with a narrow band-pass filter centered at 309 nm (FWHM = 7.6 nm) to minimize the detection of scattered light from the probe laser.[25,27] Collisional quenching of the OH($^2\Sigma_1^+$) was minimized by using helium or argon. The energies of both laser beams were measured at the exit of the reaction cell.

The resulting fluorescence signal from OH radicals detected by the PMT was integrated using a gated charge integrator over a fixed period. The delay between photolysis and probe laser pulses was varied from 10 μs to 10 ms, and the fluorescence signal (S_t) from 100 probe laser pulses at 10 Hz was averaged for each delay time to obtain the temporal profiles of the OH radical signal, which is proportional to its concentration ($[OH]_t$), see Equation 9. We usually used about 10 delay times to construct an OH-decay profile. Under pseudo-first-order conditions in [OH] ([HFO] ≫ [OH]), the following relationship is obeyed:

$$\ln\left(\frac{[OH]_t}{[OH]_0}\right) = \ln\left(\frac{S_t}{S_0}\right) = -\left(k[HFO] + k_d\right)t = -k't \qquad (9)$$

The pseudo-first-order OH decay rate coefficients in the presence (k') and absence (k_d) of HFO reactant were measured. The OH radicals are lost through reaction with HFO, as well as reaction with the OH-precursor (H_2O_2 or HNO_3) and diffusion out of the detection zone; the latter two losses were accounted for in the background removal rate coefficient, k_d.[25] $CF_3CH=CH_2$ and $CF_2HCH=CF_2$ concentration were varied over (0.19–65) and (2.8–47) × 10^{13} molecule cm^{-3}, respectively. Absolute second order rate coefficients, k (in cm^3 $molecule^{-1}$ s^{-1}), at a given temperature and pressure were obtained from the slope of the (k'-k_d) versus [HFO] variation using a linear regression procedure. They are presented at selected temperatures for $CF_3CH=CH_2$ and $CF_2HCH=CF_2$ together with experimental conditions in Tables S1 and S2.

The mixture of the OH precursor, olefin, and bath gas was flowed through the reaction cell to avoid accumulating products in the reaction volume. Calibrated mass flow controllers were employed to quantify gases flowing into the system. The temperature of the bath gas was regulated by circulating a cooling or heating fluid through the outer jacket of the reactor and measured using a retractable thermocouple (212–373 K to within ± 0.1 K). The pressure was continuously measured in the reaction cell with two calibrated pressure gauges (0–1000 Torr). Concentrations of $CF_3CH=CH_2$ and $CF_2HCH=CF_2$ were monitored online at 298 K using a 1000 cm path-length Fourier transform infrared (FTIR) spectrometer (1 cm^{-1} resolution, 500–4000 cm^{-1} range) located downstream of the LIF reactor. The integrated band strengths measured in this study (Figure S2 and S3, Table S3) were used to calculate the concentration in the reactor after correcting for pressure and temperature differences between the LIF reactor and the FTIR cell.

2.2.2. Chemicals:

All the gases used were UHP certified to be >99.9995 % (Air Liquide) pure. A 50wt.% solution of H_2O_2

was obtained from Sigma-Aldrich and concentrated before use by bubbling purified air through it for several days. $CF_3CH=CH_2$ (3,3,3-trifluoropropene) and $CF_2HCH=CF_2$ (1,1,3,3-tetrafluoropropene) were purchased from SynQuest Labs (CAS: 677-21-4, purity 99%) and (CAS: 4556-24-5, purity 98%), respectively. Two mixtures were prepared (1% and 10% in He). Purified gas-phase nitric acid was obtained by dehydrating a high-purity nitric acid HNO_3 solution (70% in H_2O) through the dropwise addition in a 1:2 ratio with concentrated sulfuric acid H_2SO_4 (>95%). Care was taken to avoid NO_2 formation in this sample over time by maintaining it at ≤0°C and preventing room air ingress; the purity was confirmed by IR spectrum analysis of the headspace.

3. Results and discussion:

3.1. SAR training set:

In this and the subsequent sections, we define the training set as those data points included in our multilinear regression analysis to derive the *F*-factors. The latter *F*-factors were optimized using a numerical solver that minimized the difference between the experimental and calculated (as defined in Equation 3) rate coefficients, as described in section 2.1.2. To test SAR performance and constrain fitting parameters, we compiled a comprehensive list of reaction rate coefficients for OH radical reactions with haloalkenes and alkenes for the training set. We used the latest version of the database of McGillen *et al.*[28] from which we obtained a total of 77 rate coefficients, 64 of which have been measured as a function of temperature (structures 1-64) and the remaining 13 determined at ~298 K (structures A-M) (Figure 2 and 3). We assume that all these data are in their high-pressure limit for an addition reaction. So far, very few alkenes have exhibited pressure dependence in their reaction with OH at pressures >100 Torr, and these appear to be limited to molecules with fewer heavy atoms such as ethene.[29] However, any rate coefficient not at its high-pressure limit would be expected to be an outlier in our correlation analysis. Furthermore, we excluded alkenes with large alkyl substituents because the OH radical could also abstract an H atom.[30]

The compounds of the training set are presented together in a single Arrhenius diagram in Figure 3. Certain rate coefficients available in the literature show non-Arrhenius behavior, which is better described by $k(T)=A\exp(-B/T)(T/300)^n$. In some cases, i.e., for (*E*)-$(CF_3)_2CFCH=CHF$, (*Z*)-1,1,1,2,3,4,4,4-octafluorobut-2-ene, (*E*)-1,1,1,2,3,4,4,4-octafluorobut-2-ene, for simplicity, we refitted such data to an Arrhenius expression for the experimental temperature range (214 to 380K for (*E*)-$(CF_3)_2CFCH=CHF$ and 230-370K for the others). The worse discrepancy between the measured data point and the value from the Arrhenius fit is observed for (*E*)-1,1,1,2,3,4,4,4-octafluorobut-2-ene at T=370 K. In that case, the re-fitted values differ from the measurements by at most 13% for compound

(*E*)-1,1,1,2,3,4,4,4-octafluorobut-2-ene over the range T=230–370 K. Although this results in a less accurate fit to the individual measurements, we consider this to have a minor effect for all the cases studied. The structures for each of the compounds considered in this study are presented in Figure 2, which are placed in order of reactivity. The selected data are divided into three groups:

1. compounds with known Arrhenius parameters (numbers 1–64)

2. compounds with only room temperature measurements (letters A–M)

3. compounds not included in the training set (grey background, see details in section 3.4.)

Since the SAR of Kwok and Atkinson as implemented in AOPWIN v1.92 includes almost all organic structures,[7-9] no additional efforts were required to extend this SAR in the present work. By contrast, the SAR of Tokuhashi and co-workers is limited to haloalkene structures.[17] We included additional alkenes and haloalkenes in the training set to extend this approach further. We opted not to include long-chain alkenes, where abstraction reactions are known to contribute to the overall reactivity.[30] Therefore, this SAR should be viewed as a quantification of the electrophilic addition reaction to the olefinic bond within a molecule rather than its overall reaction rate coefficient. However, extending this SAR to include hydrogen abstraction, similar to Kwok and Atkinson's approach,[9] would be possible.

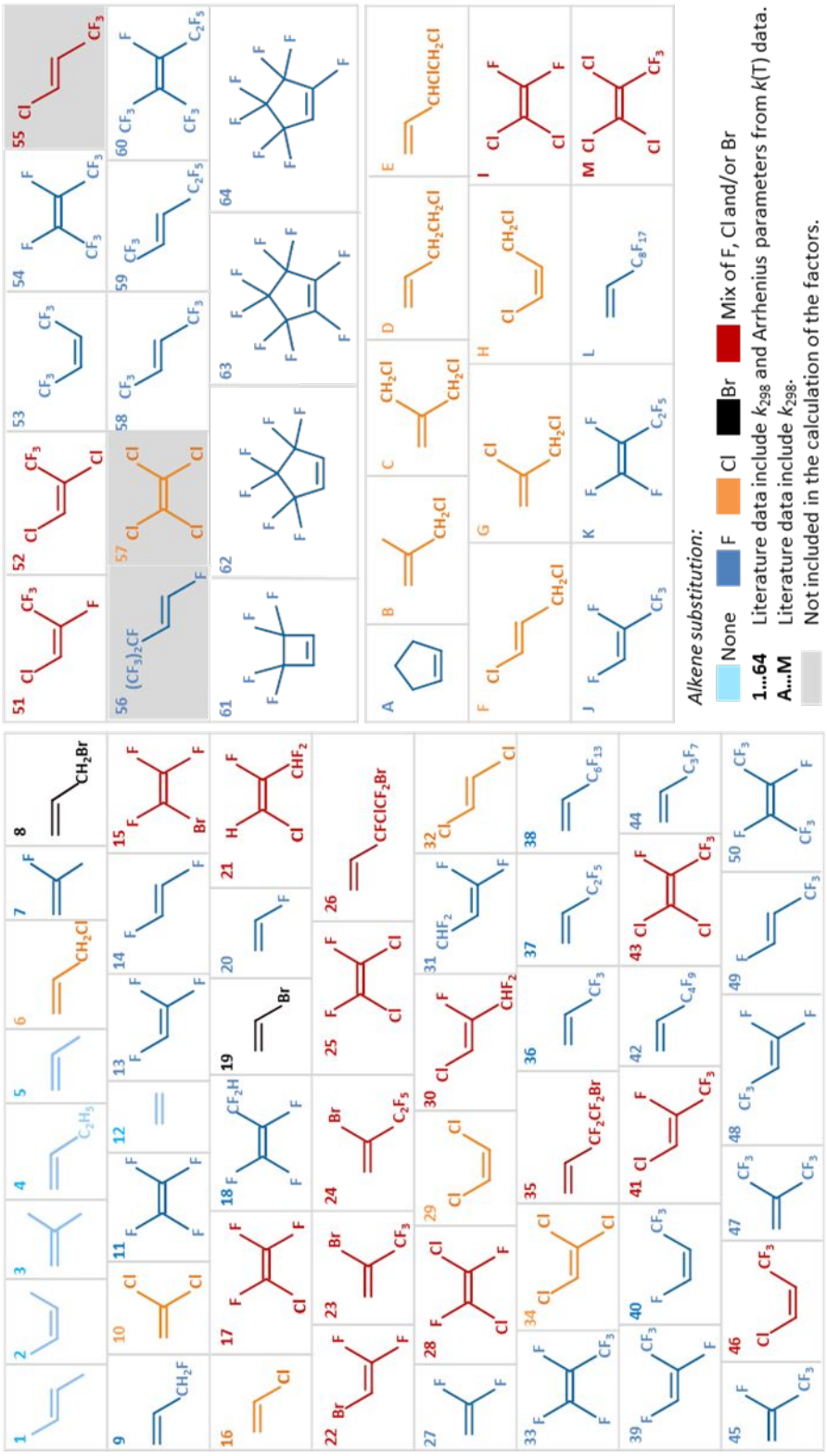

Figure 2: Structures of the 77 molecules included in this study. Molecules with $k(T)$ data (1–64) and with only k_{298} data (A–M) are ordered by reactivity at 298 K.

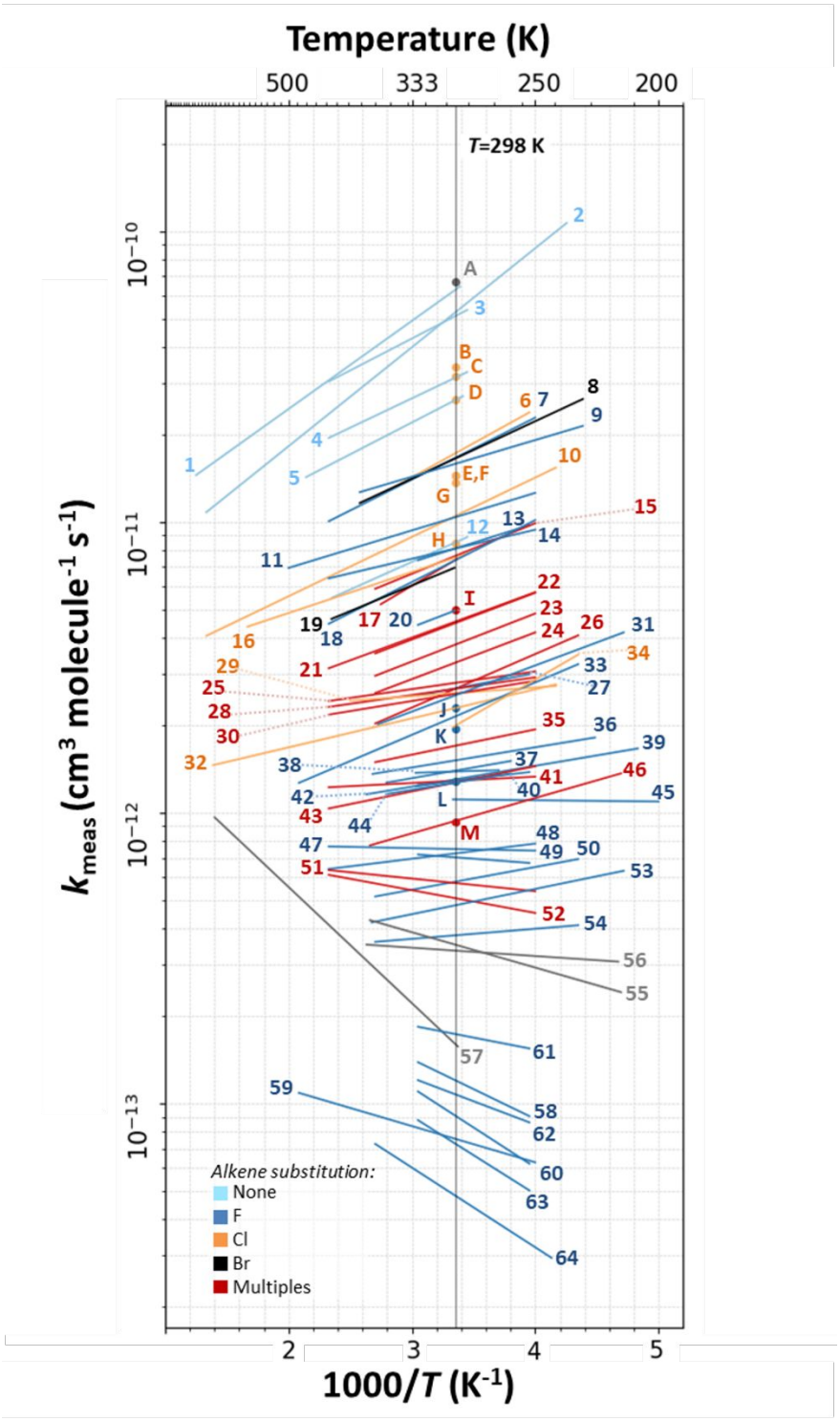

Figure 3: Arrhenius plots showing rate coefficients for all alkenes and haloalkenes included in this study. Data were taken from the recent database of McGillen *et al.*[28] Dots represent measurements at room temperature only, and lines represent temperature-dependent determinations.

3.2. Performance of SARs at 298 K:

The optimized *F*-factors of Equation 3 included in the model are displayed in Table 1. The Tokuhashi *et al.* approach[17] requires more fitting parameters than that of Kwok and Atkinson.[9] This approach, therefore, requires more data with similar structures to train the corresponding *F*-factor. As assessed in section 3.6., by adding new diagonal substituent factors in this approach, the number of rate coefficients that can be estimated has been increased, especially for longer perfluoroalkyl substitutions.

Table 1: Substituent factors optimized for the diagonal structure around the olefinic bond from this work and that of Model 1 of Tokuhashi *et al.*[17] The *F*-factors from this work are presented as defined in Equation 3. [a]Factors were optimized only from one experimental k_{298} data.

Diagonal substitutions across the double bond	**Substituent factors (*F*)**	
	This work	**Tokuhashi *et al.* (2021)**[17]
H-C=C-H	2.39	2.348
H-C=C-F	1.87	2.041
H-C=C-Cl	2.21	2.218
H-C=C-Br	5.57	Not included
H-C=C-CH_2Cl	5.62	4.971
H-C=C-CH_2Br	7.32[a]	Not included
H-C=C-CH_2F	6.69[a]	5.395[a]
H-C=C-CHF_2	2.54[a]	1.121[a]
H-C=C-C_xH_y ($x\leq2$)	9.14	7.561 for x=1
H-C=C-C_xF_y	5.93×10^{-1}	8.43×10^{-1} for x=1
H-C=C-$C_xF_yX_z$	8.57×10^{-1}	Not included
C_xH_y-C=C-C_zH_w (x=z=1)	2.64×10^{1}[a]	Not included
F-C=C-F	3.50	3.453
F-C=C-Cl	1.76	2.261
F-C=C-Br	2.28	Not included

F-C=C-CHF_2	1.69	2.109[a]
F-C=C-C_xF_y	5.54×10^{-1}	3.84×10^{-1} for x=1
Cl-C=C-Cl	9.04×10^{-1}	5.79×10^{-1}
Cl-C=C-CHF_2	1.36	2.194[a]
Cl-C=C-C_xF_y	7.20×10^{-1}	2.94×10^{-1} for x=1
C_xF_y-C=C-C_xF_y	7.78×10^{-2}	Not included
Cl-C=C-CH_2Cl	6.02[a]	6.132[a]
F_{cycle}	3.07×10^{-1} (cyclic) 1 (acyclic)	Not included

The performance of the SARs of Kwok and Atkinson,[9] the SAR of Tokuhashi *et al.*,[17] and our extension of the SAR of Tokuhashi *et al.* was assessed at 298 K. A comparison between calculated rate coefficients and experimental measurements is shown in Figure 4 for each of these methods. The SAR of Kwok and Atkinson,[9] the original SAR formulation, was found to be notably less accurate than the other methods, as 64% of the training set predictions are under- or overestimated by more than 50%, with many outliers being up to 2 orders of magnitude larger or smaller than the measured values. For example, one estimate is 400 times larger than the measurement, i.e., for (*E*)-$CF_3CH=CHCF_2CF_3$ with $k_{meas} = 9.10 \times 10^{-14}$ cm^3 $molecule^{-1}$ s^{-1} and $k_{calc} = 3.70 \times 10^{-11}$ cm^3 $molecule^{-1}$ s^{-1}. There are several potential reasons for the discrepancy. It could be a limitation in the algorithm itself, demonstrating a high degree of degeneracy towards certain structural attributes. We define this degeneracy as various substitution patterns yielding identical rate coefficients (see Figure 4). Furthermore, the method provides the same estimates for rate coefficients measured to be 2 orders of magnitude apart from each other, *cf.* $CF_2=CF_2$ ($k_{meas} = 1.04 \times 10^{-11}$ cm3 $molecule^{-1}$ s^{-1}) versus $CCl_2=CCl_2$ ($k_{meas} = 1.60 \times 10^{-13}$ cm^3 $molecule^{-1}$ s^{-1}) both of which are estimated to have a rate coefficient of $k_{calc} = 2.14 \times 10^{-13}$ cm^3 $molecule^{-1}$ s^{-1}. As discussed in more detail in section 3.6, the predictions and measured values agree in our approach. The increased number of fitting parameters in the Tokuhashi method[17] and our extended version affords the individual prediction of rate coefficients for specific isomeric structures, which is one of the reasons why degeneracy is lower in these approaches compared to the Atkinson method.[9-12]

We note that difficulties with multiple substituted haloalkenes have been recognized since the inception of this approach.[9-12] In addition, the training set available for the current implementation of the Kwok and Atkinson method[9] was limited compared to the Tokuhashi approach[17] presented here. Rate coefficients at room temperature, k_{298}, were well-predicted using the modified Tokuhashi approach, as

illustrated in Figure 4. Tokuhashi's SAR[13,17] and our extended version show only minor differences, with 80% and 77%, respectively, of cases being reproducible to within a factor of 2. Our approach to generalizing the SAR to include more haloalkenes and alkenes appears not to come at the cost of reducing its overall performance.

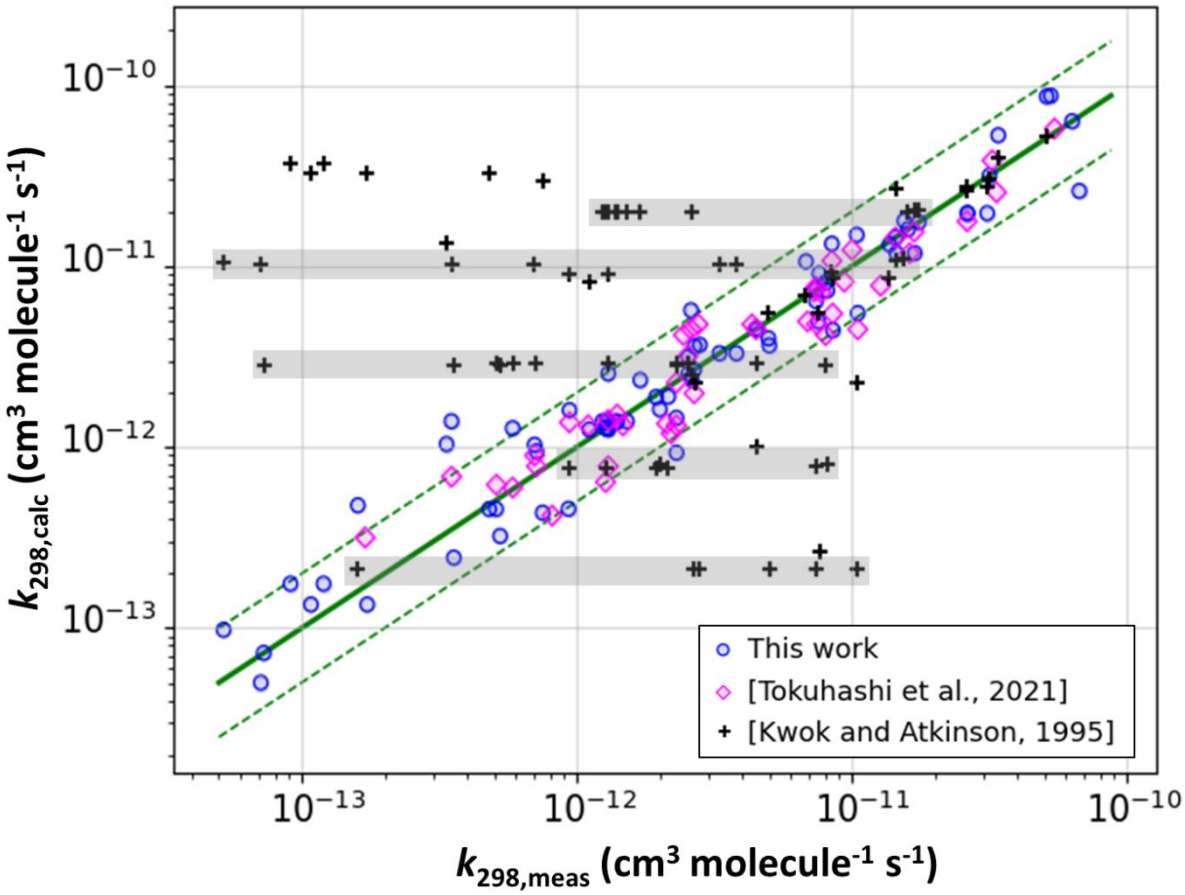

Figure 4: SAR results and comparison with Tokuhashi predictions[17] (magenta diamond) and AOPWIN[7,8] calculations based on Kwok and Atkinson approach[9] (black plus) at 298 K. Blue circles are predictions using our SAR model ($k_{298,calc}$). Green dashed and bold lines show the interval in which data calculated agree within a factor of 2 with measured data. The grey areas indicate identical predictions from AOPWIN as a consequence of the degeneracy in the SAR algorithm.

3.3. The relationship between k_{298} and E_a/R:

Next, we investigated the effect of temperature on alkene and haloalkene reaction rate coefficients. By comparing all temperature dependencies in a single Arrhenius diagram (see Figure 3), it is clear that the experimental temperature dependence factor (E_a/R) switches from a positive to a negative value as the

rate coefficient at 298 K becomes larger. By correlating the experimental E_a/R with the $\ln(k_{298})$ (Figure 5), we found that the data could be fitted adequately using an inverse sigmoidal function for E_a/R ranging from -784 K to +920 K, as:

$$\ln\left(\frac{k_{298}}{2.7 \times 10^{-10}}\right) = \frac{\text{-8.6}}{\left[1 + \exp\left(\frac{\text{-300 K} - \frac{E_a}{R}}{\text{363 K}}\right)\right]} \qquad (10)$$

where $\ln(k_{298})$ is the natural logarithm of the room temperature rate coefficient k_{298} in cm^3 $molecule^{-1}$ s^{-1}, and E_a/R is the Arrhenius activation energy in Kelvins, both of which are measured properties. The remaining values represent optimized fitting parameters. Equation 10 is a parametrization function and does not provide physical meanings for the parameters. Reactions with the lowest activation energies possess rate coefficients close to their collision limits, resulting in a lower limit in E_a/R factors.

Although it should be remembered that the exact size of the collision rate coefficient will vary depending on several parameters such as the size or the polarizability of the molecules involved. Nevertheless, the probability of collision between the OH radical and the olefinic bond is unlikely to change drastically within the training set.

Conversely, the less reactive compounds will possess the highest E_a value. It is intuitive to expect a limit to which a given selection of halogenated substitutions can withdraw electrons from the olefinic bond, e.g., in perfluoroolefins. Indeed, similar E_a/R values are seen for the less reactive molecules in this study. Hence, the lower bound of the fit is assumed to be equal to the lowest measured value of E_a included in this training set.

These upper and lower bounds ($(E_a/R)_{min}$ = -784 K and $(E_a/R)_{max}$ = +920 K) therefore bracket the range of values that we encountered in this training set. In the following steps of the calculation, for k_{298} larger than 7.3×10^{-11} cm^3 $molecule^{-1}$ s^{-1} and smaller than 2.3×10^{-14} cm^3 $molecule^{-1}$ s^{-1}, the calculated E_a/R factors were forced to be equal to the upper and lower bounds of the fit respectively (Figure 6).

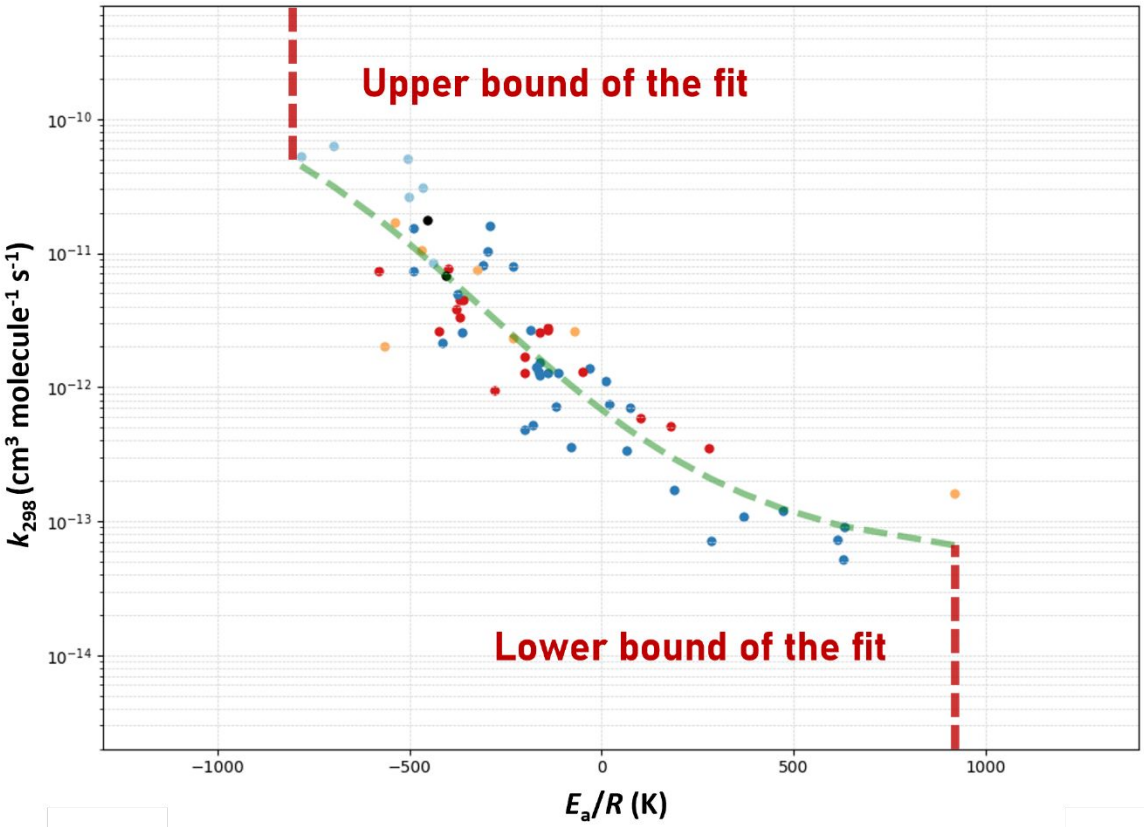

Figure 5: Inverse sigmoidal fit of k_{298} vs. E_a/R for all the 77 molecules included in this study and described in Figure 2.

3.4. Extension and performance of SAR for temperature dependence between 200 and 400 K:

The A-factor (in cm^3 molecule^{-1} s^{-1}) has been calculated to extend the room temperature predictions to temperature-dependent ones. As seen in Table S4 and Figure S4, A-factor in our training set can range from 1.98×10^{-13} cm^3 molecule^{-1} s^{-1} to 9.42×10^{-12} cm^3 molecule^{-1} s^{-1}. Hence, to account for its variation, the A-factor was retrieved using the estimated k_{298} (Equation 3) and the estimated E_a/R factor (Equation 10) using the equation:

$$A = k_{298} \exp\left(\frac{Ea}{298 \times R}\right) \quad (11)$$

Then, Arrhenius parameters and $k(T)$ can be estimated over the temperature range of this study (200–400 K); the results are plotted in Figure 6. The agreement between measurements and calculations $k_{calc}(T)$ is quantified from the ratio relative to the measured values $k_{meas}(T)$, defined as k_{calc}/k_{meas} when $k_{calc} > k_{meas}$ and k_{meas}/k_{calc} when $k_{meas} > k_{calc}$, in Figure 7. In general, temperature-dependence is well-predicted using this method. Most (~84%) of the predicted rate coefficients are within a factor of two of

the experimental values throughout the temperature range of 200 to 400 K, as presented in Figure 8.

Three notable exceptions are CCl_2=CCl_2, (*E*)-CHCl=$CHCF_3$, and (*E*)-$(CF_3)_2$CFCH=CHF, where the predicted rate coefficients are higher than those measured. These compounds were excluded from the fitting procedure as they demonstrated no apparent improvement when optimizing the *F*-factors. All three of these molecules possess a high degree of halogenation, with two of them containing chlorine. Tokuhashi *et al*.[17] have observed previously that chlorination results in worse predictions. It can either be because of a mechanistic difference that this SAR does not adequately describe chlorinated molecules or due to some significant uncertainties and disagreements in the experimental data. We are not yet able to understand the exact reason for this behavior.

For highly halogenated compounds, multiple halogen substitutions and the specific bulkiness of chlorine substitutions close to the reactive center (i.e., the olefinic bond) may contribute to the steric strain and steric shielding that is encountered in the electrophilic addition.[31] Furthermore, since these are electrophilic addition reactions, we expect the electron withdrawal in the π-orbitals to have an important effect on the overall rate coefficients. Specific combinations of halogen substitutions within a sidechain may also influence reactivity. In the example of (*E*)-$(CF_3)_2$CFCH=CHF, the $(CF_3)_2$CF- substitution may have a more potent electron-withdrawing effect than the generic CF_2X-, to which we have assigned it. Evidence for such an influence comes from the resonance and field parameters which are notably different from the straight-chain perhalogenated substitutions,[32] and which could be responsible for the low reactivity of (*E*)-$(CF_3)_2$CFCH=CHF towards OH. However, further theoretical work and measurements are required to better understand the mechanisms of these reactions.

There is also the possibility that there may be some mechanistic differences for some of the reactions contained within our dataset. This would explain why some rate coefficients are poorly predicted using this SAR approach, since one of the main assumptions of this work is that all reactions considered here are governed by the same structural attributes.

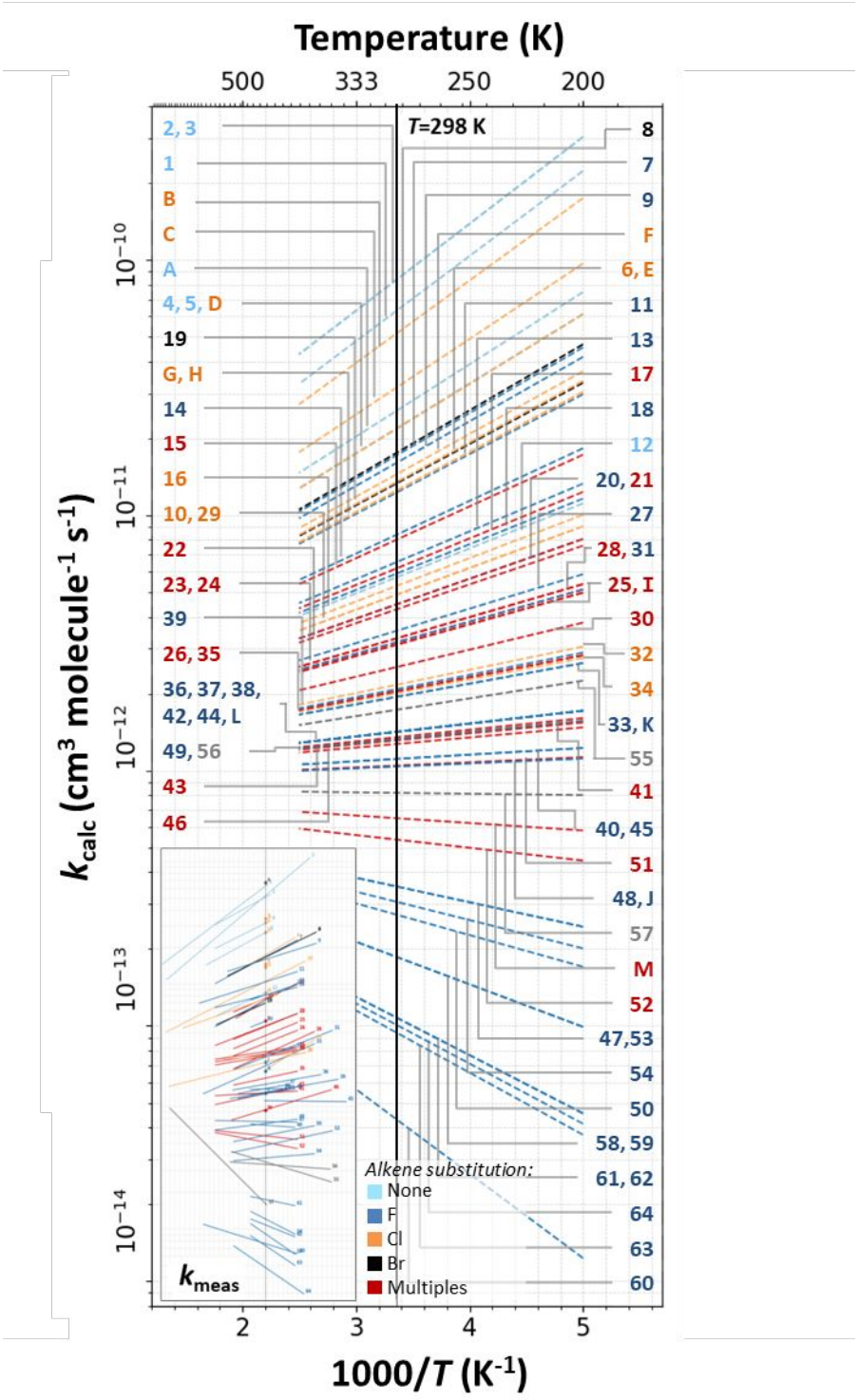

374

375 **Figure 6:** Experimental data (inset) and predictions of $k_{calc}(T)$ over the studied temperature range (200−400 K) in
376 dashed lines using our SAR model. Experimental values are plotted from Arrhenius parameters McGillen *et al.* in
377 bold lines.[28]

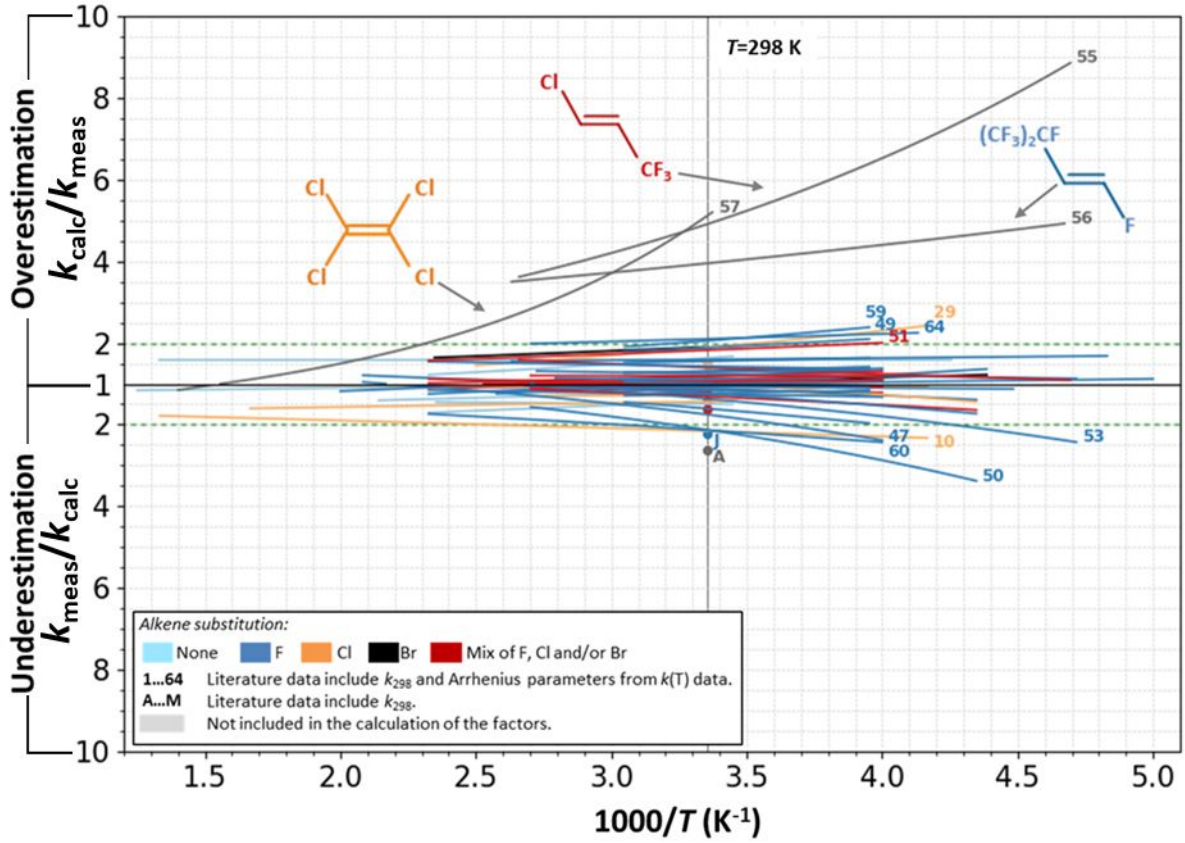

Figure 7: Ratio between measured and calculated rate coefficients over the temperature range of this study, is defined as k_{calc}/k_{meas} when $k_{calc} > k_{meas}$ and k_{meas}/k_{calc} when $k_{meas} > k_{calc}$. Green dashed and bold lines showing the interval in which data calculated agree within a factor 2 with measured data.

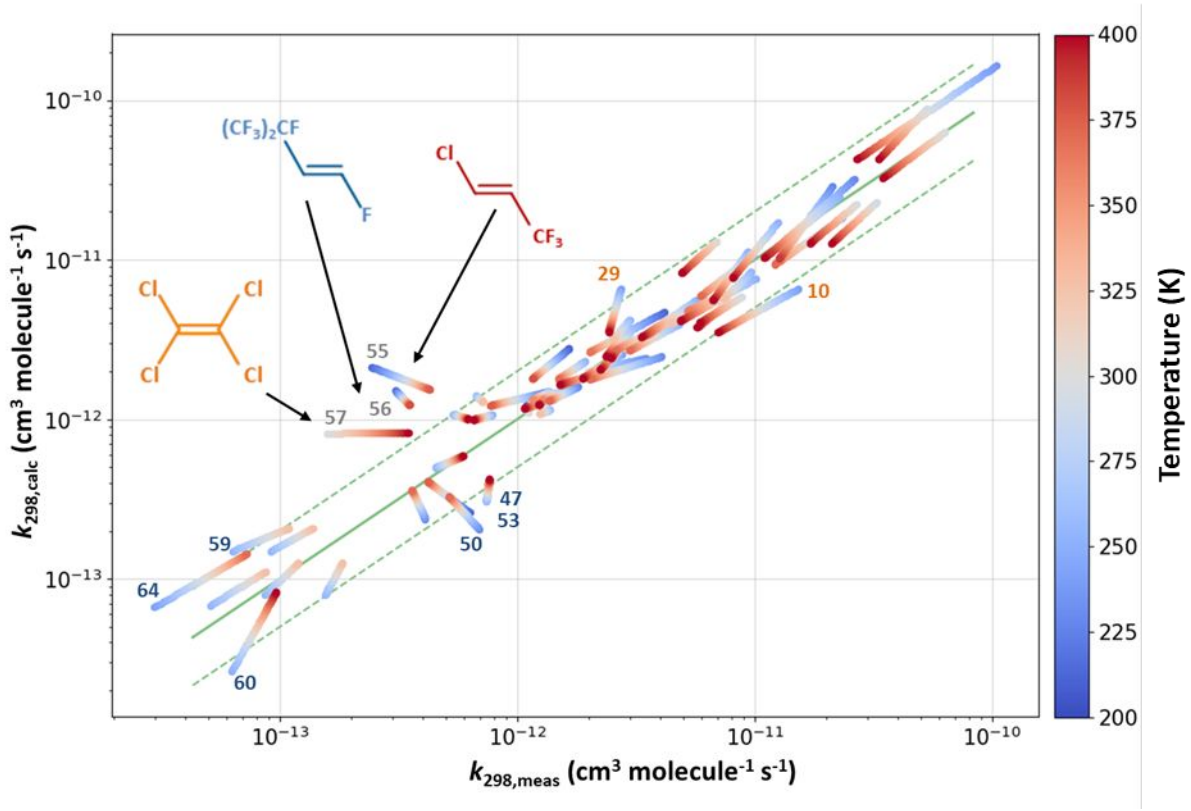

Figure 8: Calculated OH rate coefficients versus measured OH reaction rate coefficients as a function of temperature over 200–400K. The bold green line represents the perfect agreement between prediction and measurements. The dashed lines identify the range within which calculations and measurements agree within a factor of 2 on either side.

3.5. Measurements of the temperature dependence for the reaction rate coefficients of OH with $CF_3CH=CH_2$ and $CF_2HCH=CF_2$:

To test the SAR for predicting the temperature dependence, we determined the Arrhenius parameters and k_{298} for the reaction of OH with $CF_2HCH=CF_2$ between 223 and 373 K using our PLP–LIF setup. There are no experimental data available for this reaction. In addition, we measured the established rate coefficient for OH reaction with $CF_3CH=CH_2$ (212–367 K).

The measured values of the OH reaction rate coefficient as a function of temperature for the two selected HFOs, $CF_3CH=CH_2$ and $CF_2HCH=CF_2$, are provided in Tables S1 and S2, respectively, together with the experimental conditions. The pseudo-first-order decay rate coefficients of the OH fluorescence signal k' (s^{-1}), are plotted against the concentration of the HFO (in molecule cm^{-3}), yielding second-order plots, examples of which are shown in Figure 9. The slopes of the lines give the OH reaction rate coefficients k (cm^3 $molecule^{-1}$ s^{-1}) based on Equation 9. The reported uncertainties in the

rate coefficient determinations reflect the statistical uncertainties (2σ at 95% CI) from the uncertainty-weighted linear least squares fit of these data. The overall systematic errors of the measurements were estimated to be <15%, including statistical error in k' (<6%) and temperature (1%), and the estimated uncertainty in the concentration of HFO (~10%) and pressure (~6%). Flow rates and concentrations of gases were varied from one run to another to test the reproducibility of our results. The use of nitric acid or hydrogen peroxide as precursors for OH radicals displayed no noticeable difference in the measured rate coefficients. The linearity in the second-order plots indicates that the pseudo-first-order assumption remains valid in our experimental conditions.

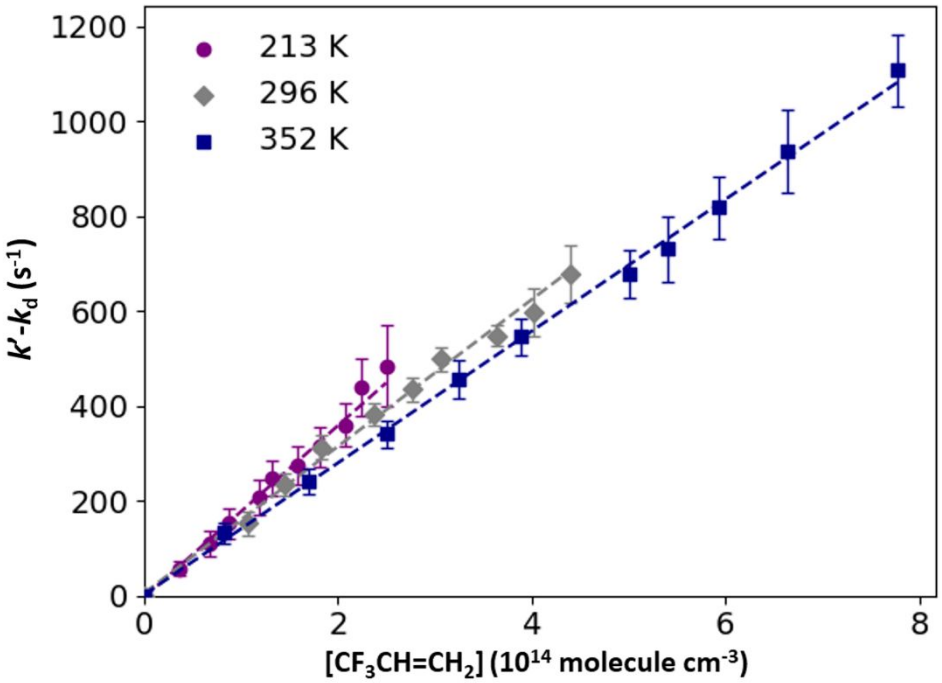

Figure 9: Representative plots of the dependence of the pseudo-first-order rate coefficient (k') on [$CF_3CH=CH_2$] at three temperatures measured using the PLP−LIF apparatus. Plotted uncertainties represent statistical errors (2σ at 95% CI).

The temperature-dependence of the reaction rate coefficients for $CF_3CH=CH_2$ between 212 and 367 K and $CF_2HCH=CF_2$ between 223 and 373 K were well represented by a simple Arrhenius expression (see Figure 10). Both reactions exhibit negative temperature dependencies. To obtain the Arrhenius parameters, we employed an uncertainty-weighted linear least squares curve-fitting routine to the logarithm of the temperature-dependent rate coefficient data, $\ln(k_{298})$, as a function of inverse temperature, using the reported statistical uncertainties of the experimental data. The parameters from this work and the literature are presented in Table 2, and the Arrhenius plots are shown in Figure 10.

The fits of our experimental data are defined as follows:

$$k_{OH + CF_3CH=CH_2}(T) = (8.4 \pm 1.3) \times 10^{-13} \exp\left(\frac{161 \pm 12}{T}\right) \quad (12)$$

and

$$k_{OH + CF_2HCH=CF_2}(T) = (7.6 \pm 1.2) \times 10^{-13} \exp\left(\frac{365 \pm 6}{T}\right) \quad (13)$$

where the stated uncertainties represent the combined absolute and statistical errors (2σ at 95% CI) of the measurements. We compare our results for OH reaction with $CF_3CH=CH_2$ with the measurements and the associated uncertainties of Tokuhashi *et al.,*[13] Orkin *et al.,*[18] and González *et al.* in Figure 10.[22] The plotted uncertainties of k for the literature data represent only statistical errors. Our results are in excellent agreement with the data from Orkin *et al.*,[18] and only slightly different from those of González *et al.*[22] and Tokuhashi *et al.*[13] at lower temperatures. To the best of our knowledge, we are the first to report the rate coefficients for reaction with $CF_2HCH=CF_2$. Compared to $CF_3CH=CH_2$, the reactivity of $CF_2HCH=CF_2$ is higher, with a larger negative temperature dependence. This was also anticipated by the relationship between k_{298} and E_a/R (see Figure 5). We have extended the minimum temperature for which data are available in the literature, from 250 to 212 K, in OH rate coefficient determinations for the reaction with $CF_3CH=CH_2$.[13]

The parameters predicted from the model are in good agreement with the measured values (Figure 10 and Table 2), with k_{298} underpredicted for $CF_3CH=CH_2$ by only 7% and overpredicted for $CF_2HCH=CF_2$ by 24%. One of the diagonal substituent factors of the newly measured $CF_2HCH=CF_2$, F(F-C=C-CF_2H), was trained with only one other compound in the model, which explains the lower accuracy compared with the more studied F(H-C=C-CF_3) present in $CF_3CH=CH_2$. To improve the model, we then re-evaluated the F-factors, including k_{298} for $CF_2HCH=CF_2$ we measured in this work, and, as expected, notable improvements can be observed (see red/green plots in Figure 10).

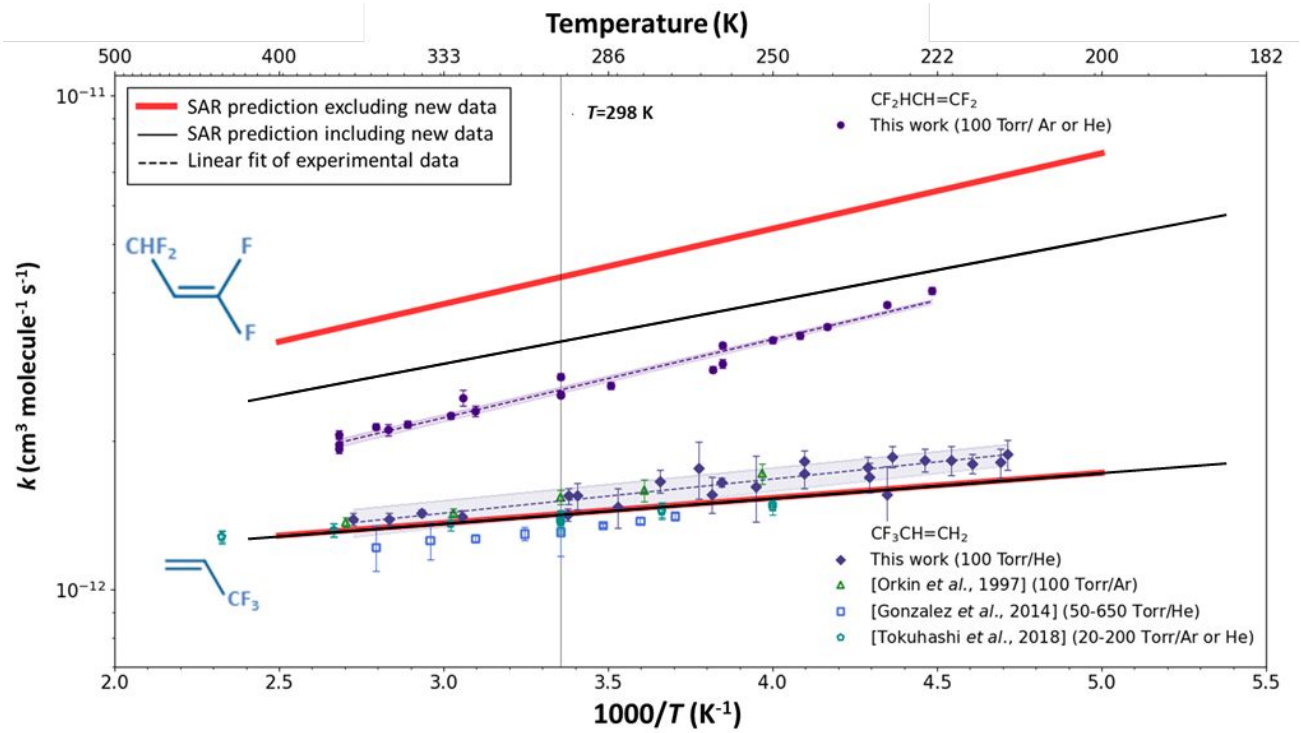

Figure 10: Arrhenius plots on a log scale showing the experimental measurements of the $k(T)$ as a function of inverse temperature, $1000/T$, for the reaction of OH radicals with $CF_3CH{=}CH_2$ and $CF_2HCH{=}CF_2$ measured in this work, compared to the literature.[13,18,22] SAR predictions from the model without including the new measurements presented in this work are plotted in red, while the updated version that includes the new data is plotted in black. A notable improvement in the prediction of OH rate coefficient for the reaction with $CF_2HCH{=}CF_2$ is observed, whose diagonal factors were constrained by only one previous measurement.

Table 2: Arrhenius parameters for reactions of OH with $CF_3CH{=}CH_2$ and $CF_2HCH{=}CF_2$ compiled from this work and previous studies.[13,18-23] For $CF_3CH{=}CH_2$, the recommendation of Arrhenius parameters results from the fit including data of this work and that of Orkin *et al.*,[18] while k_{298} is a weighted average of all the rate coefficients reported in the literature. P is the total pressure of the carrier gas (He or Ar) and reactive compound. The quoted error bars are those of the authors. [a]FP: flash photolysis, RF: resonance fluorescence, RR: relative rate methods. [b]Reported values for A, E_a/R, and k_{298} in the table are the SAR predictions when including new measurements for $CF_3CH{=}CH_2$ and $CF_2HCH{=}CF_2$. For comparison, the values of (A, E_a/R, k_{298}) predicted from the SAR before adding the new measurements are (1.32×10^{-12} cm^3 molecule^{-1} s^{-1}, 351 K, 4.28×10^{-12} cm^3 molecule^{-1} s^{-1}) for $CF_2HCH{=}CF_2$ and (9.61×10^{-13} cm^3 molecule^{-1} s^{-1}, 117 K, 1.43×10^{-12} cm^3 molecule^{-1} s^{-1}) for $CF_3CH{=}CH_2$.

Molecule	A (10^{-13} cm^3 molecule^{-1} s^{-1})	E_a/R (K)	k_{298} (10^{-12} cm^3 molecule^{-1} s^{-1})	T (K)	P (Torr)	Technique[a]	Reference
$CF_3CH=CH_2$	9.60	116	1.42	200–400		Calculations[b]	This work
			1.51	298		Calculations	(Tokuhashi *et al.,* 2021)[13]
	8.86 ± 0.82	159 ± 26	1.47 ± 0.25	212–367	100	PLP–LIF	This work
	8.28 ± 0.7	183 ± 26	1.52 ± 0.02	252–370	100	FP–RF	(Orkin *et al.,* 1997)[18]
	7.65 ± 0.26	165 ± 10	1.31 ± 0.14	263–358	50–650	PLP–LIF	(González *et al.*, 2015)[22]
	10.6 ± 0.20	80 ± 10	1.40 ± 0.01	250–430	20–200	FP, PLP–LIF	(Tokuhashi *et al.*, 2018a)[13]
			1.36 ± 0.25	296	700	RR	(Andersen *et al.*, 2005)[19]
	8.86 ± 0.71	**160 ± 24**	**1.40 ± 0.67**				**Recommendation**
$CF_2HCH=CF_2$	12.0	290	3.17	200–400		Calculations[b]	This work
	7.46 ± 0.34	365 ± 13	2.55 ± 0.18	223–373	100	PLP–LIF	This work

3.6. Discussion of the SAR:

In this section, we discuss the degeneracy in the predictions from our SAR and other existing methods as the number of isomers increases. We begin by enumerating all isomers of alkenes, N_{tot}, and haloalkenes containing C, H, F, Cl, and Br up to a carbon number of 4. We obtained N_{tot} using a set of Markush structures generated in MarvinSketch version 22.5.0, ChemAxon (https://www.chemaxon.com). Since AOPWIN outputs distinctively H-abstraction and OH-addition reaction rate coefficients, to test the degeneracy of this method with regards to the electrophilic addition, we filtered this output to exclude the contribution of H-abstraction reaction channels in this section and only use OH addition reaction rate coefficients. Taking this into account, we computed OH electrophilic addition reaction rate coefficients, $k_{add,}$ for all the possible isomers using the AOPWIN program. We eliminated duplicates to obtain the number of unique predictions, N_{pred}, for each carbon number. Similarly, we enumerated all the unique predictions of k_{298} that can be obtained with the diagonal factors given in this work. The comparison between the number of existing isomers and the number of unique predictions from each approach is presented in Figure 11. It is noted that within these enumerations, optical isomers will be present, and this form of isomerization is not expected to impart a change to the rate coefficient.

There are many possible structures with all combinations of halogens and alkenes (Figure 11). So far, the substituted ethenes alone constitute 76 isomers. As the number of carbons increases, the number of isomers increases exponentially, many of which are of potential interest in various applications. It would be impractical to measure each one or even calculate them all with theory. SARs provide a rapid way to

estimate all these possibilities. Since it is a simplification, we can expect uncertainties in these predictions (Figure 11, Panel a). We observed significant degeneracy in the predictions of AOPWIN (see trends of similar *k*-values in Figure 4), although in this case, the *k*-values include both the OH addition and the H-abstraction pathways. Here, we only compare the OH electrophilic addition rate coefficient values, and we observe an important degeneracy again in the estimations of AOPWIN (Figure 12). For example, at a carbon number of 2, there are 76 isomers and, in the best case, 36 unique predictions are obtained from this SAR. But as the carbon number increases, the number of unique predictions grows slowly relative to the number of possible isomers (Figure 11, Panel b). For clarity, we only present our SAR predictions together with those of AOPWIN as our algorithm is only an extension of the approach of Tokuhashi *et al*.,[17] and hence the level of degeneracy and distribution of predictions is similar.

Our description above raises the question: how simple is too simple? Inspecting the currently available dataset, one can observe that the dataset of reaction rate coefficients is quite evenly distributed (Figure 12). Based on the available data in the training set, there does not seem to be a dominant mode in the rate coefficient distribution, overall, it looks almost continuous. The estimation space of our approach appears to be more uniformly distributed compared to the AOPWIN program, which has several clusters of degenerate predictions. For example, the clusters 56 and 82 (x-axis) out of the 100 *k*-data groups in Figure 12 contain the highest frequencies of predictions from AOPWIN, meaning that there are many estimates having the same rate coefficient, even though there are no or few experimental data in this range. This highlights both the problem of degeneracy and inaccuracy when using a SAR. This work improves upon previous methods since it appears to reproduce and cover the entire distribution uniformly, consistent with the pattern of the experimental data.

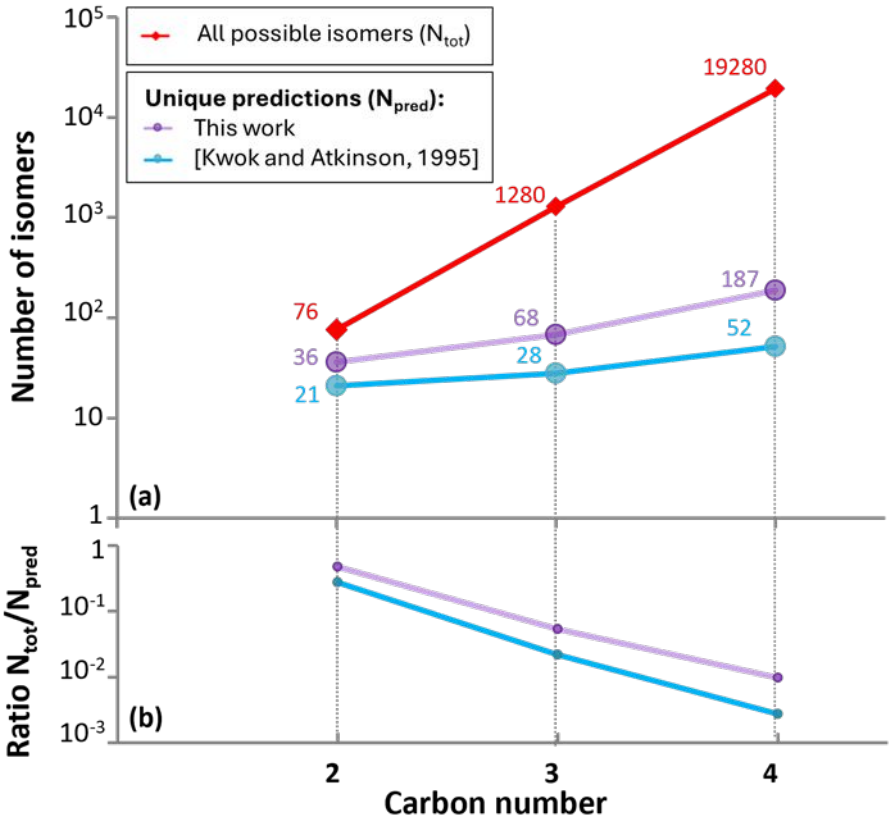

Figure 11: Panel a: Number of possible olefinic isomers from the combination of H, F, Cl, and Br substitutions at carbon numbers between 2 and 4, N_{tot}, in relation to the number of unique predictions, N_{pred}, obtained with the approaches of Kwok and Atkinson[9] obtained from AOPWIN and this work. Panel b: Ratio between N_{tot} and N_{pred}.

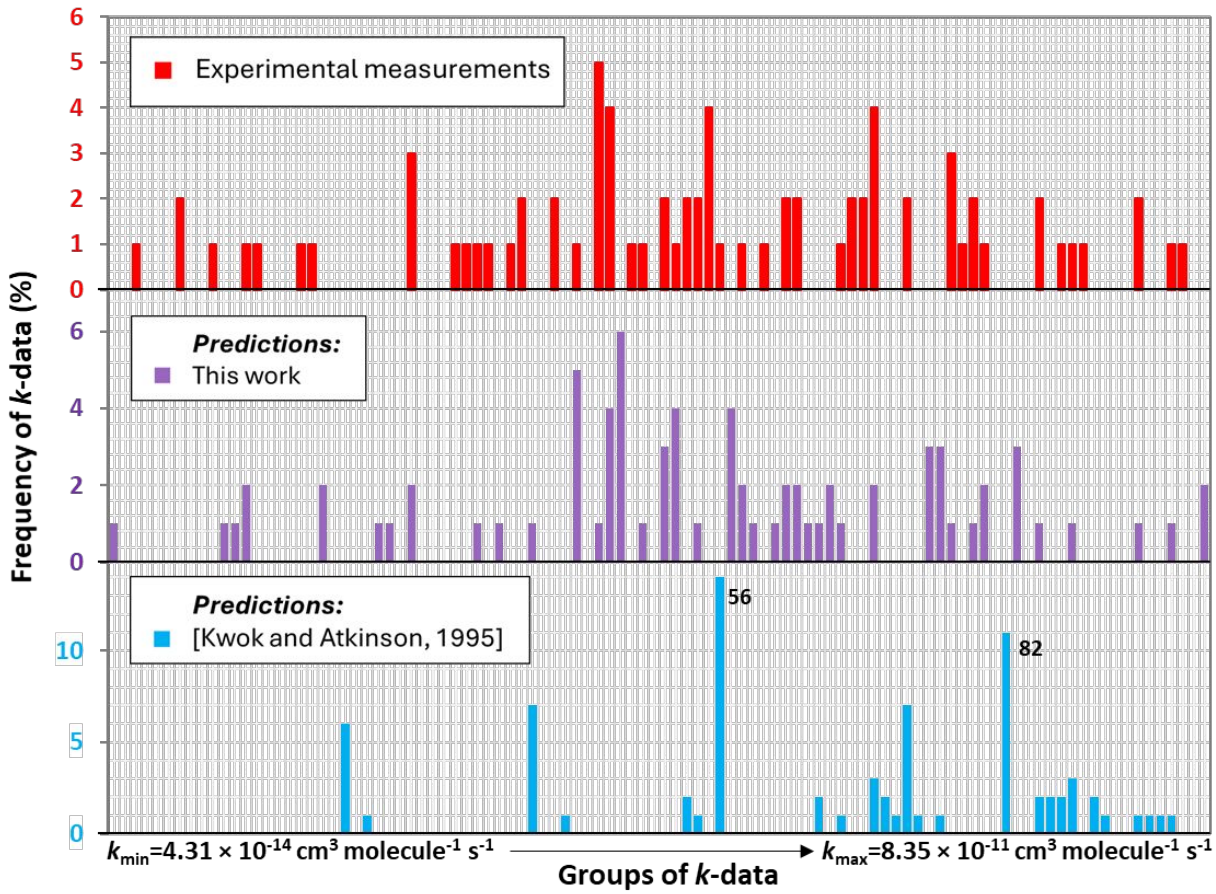

Figure 12: Histograms of the available kinetic data for the OH reaction with alkenes of interest. Upper panel: the measured rate coefficients, Middle panel: values calculated from this work, Lower panel: values calculated with the approach of Kwok and Atkinson[9] outputted from AOPWIN. Rate coefficients are binned into 100 groups of evenly distributed k_{298}-rate coefficients ranging from the minimum k_{298} through to the maximum.

3.7. Atmospheric implications:

Most of the haloalkenes of this training set are short-lived, and thus they are not well mixed in the troposphere. Their lifetimes depend strongly on the location and time of their emission.[33,34] An average tropospheric lifetime calculation would not be accurate for all cases. By estimating reaction rate coefficients with this method, one can then evaluate the tropospheric lifetime of the compound of interest using the approach of Brioude *et al*.[33] Consequently, rather than focus on the tropospheric lifetime of each compound, we explore the potential of SARs in their use as a screening tool. Rapid and straightforward estimation of the OH reaction rate coefficient for a large number of haloalkenes is possible using this approach, allowing scientists, industries, and policymakers to select more environmentally friendly product candidates conveniently.

4. Summary and Conclusions:

In this work, we developed a method to predict the Arrhenius parameters of the OH addition reaction rate coefficients of haloalkenes and related compounds. For this purpose, we used literature data for the OH kinetics of hydrofluoroolefins (HFOs) and related haloalkenes, constituting the training set of this study. From the structure-activity relationship (SAR) of the OH rate coefficients of this training set, a trend was observed between reactivity, structure, and activation energy. The more reactive compounds ($k_{298} \sim 10^{-12}$–10^{-10} cm^3 molecule^{-1} s^{-1}) have a predominantly negative temperature dependence, while less reactive compounds ($k_{298} \sim 10^{-12}$–10^{-14} cm^3 molecule^{-1} s^{-1}) display a generally positive temperature dependence. This is consistent with the expectation that the barrier for a reaction hinders reactivity for many compounds. Our method to calculate room-temperature reaction rate coefficients, k_{298}, is in good agreement with measurements as well as previous approaches developed by Tokuhashi *et al.*[17] and Kwok and Atkinson,[9] as more recently implemented in the AOPWIN program, as described in Lim's paper.[7,8] The extended method we present to predict $k(T)$ over the temperature range 200–400 K is the first temperature-dependent calculation method to predict the kinetics of OH-addition to haloalkenes. The overall performance of this new approach was found to be satisfactory, as 90% of the estimated Arrhenius parameters agree within a factor of 2 for the 77 compounds examined. Our method provides an excellent starting point for estimating the temperature-dependent OH electrophilic addition rate coefficient for a wide range of halogenated alkenes as a multiplication of three *F*-factors developed in this work.

This approach is built upon the simplest possibility that these *F*-factors are proportional to the reactivity of the double bond. The multiplicative substituent factors, *F*(X-C=C-Y) and *F*(Z-C=C-W), may relate to, amongst other possible factors, the electron density of the π-orbital of the double bond of the compounds. The lower the value of the diagonal substitution factor, the lower the electron density, and the higher the diagonal substitution factor, the larger the reactivity. Additional steric effects could be involved for the cyclic structures compared to the linear structures, which could change their reactivity. These effects are captured by the additional multiplicative F_{cycle} factor. We observe a commonality among all the alkenes we consider, suggesting that the mechanism is essentially the same without abrupt changes within the training set. There are potential exceptions in the case of certain chlorinated compounds. We interpret the common pattern in the training set to mean that the electrophilic OH oxidation of each of these alkenes is essentially similar.

We also report measurements of the OH reaction rate coefficient as a function of temperature of two HFOs, $CF_3CH=CH_2$ (212–367 K) and $CF_2HCH=CF_2$ (223–373 K), obtained using the PLP–LIF technique. Our $k(T)$ measurements for $CF_3CH=CH_2$ are in good agreement with those reported in the literature, with the range of temperature range being extended in this study. Measurements of

$CF_2HCH=CF_2$ kinetics are the first available to date and are in good agreement with the predictions obtained from our SAR. The measurements of the latter compound helped refine the parameterization of the CF_2H functionality, which was poorly represented before.

These predictions represent an improvement in predicting the rate coefficients of haloalkene degradation with the OH radical. The value of this work lies in advancing our ability to easily and quickly estimate the rate coefficient for OH reactions with at least 291 haloalkenes, among which 214 compounds have no experimental data reported so far. A significant improvement has been observed in reducing degeneracy in the estimates and increasing the variety of predictable structures compared to previous existing methods. This provides a tool that industries and policymakers can easily use to select the most reactive molecules among the different possible compounds that could be implemented as new substitutes to help avoid atmospherically persistent emissions and estimate their potential to produce local ozone.

Supplementary Material:

Excel data file: DATA-SI.csv and .xslx with all the data for reaction rate coefficients and Arrhenius parameters from existing measurements and calculations from this work, Tokuhashi and co-workers[13-17] and the AOPWIN program[7,8].

Figure S1: Schematic diagram of the pulsed-laser photolysis–laser-induced fluorescence (PLP–LIF) experimental setup.

Table S1: Experimental conditions and parameters of the absolute rate measurements of the reaction of OH radicals with $CF_3CH=CH_2$ using the pulsed-laser photolysis–laser-induced fluorescence (PLP–LIF) setup.

Table S2: Experimental conditions and parameters of the absolute rate measurements of the reaction of OH radicals with $CF_2HCH=CF_2$ using the pulsed-laser photolysis–laser-induced fluorescence (PLP–LIF) setup.

Figure S2: Typical Beer-Lambert plot showing the integrated band strength (IBS) as a function of $CHF_2CH=CF_2$ concentration, at the wavenumber range used to obtain [$CHF_2CH=CF_2$] in OH kinetic analysis.

Figure S3: Typical Beer-Lambert plot showing the integrated band strength (IBS) as a function of $CF_3CH=CH_2$ concentration, at the wavenumber range used to obtain [$CHF_2CH=CF_2$] in OH kinetic analysis.

Table S3: $CHF_2CH=CF_2$ and $CF_3CH=CH_2$ integrated band strengths, $S_{int,}$ measured at wavenumber

ranges relevant to the atmospheric window using manometrically prepared mixtures in He, ideal gas and Beer-Lambert laws.

Table S4: Results of the $k(T)$ predictions using the model with factors in Table 1.

Figure S4: Reaction rate constant at room temperature k_{298} as a function of the Arrhenius A-factor.

Acknowledgments:

This work is supported by Labex Voltaire (ANR-10-LABX-100-01), the European Union's Horizon 2020 research and innovation programme through the EUROCHAMP-2020 Infrastructure Activity under grant agreement No. 730997, and Le Studium Loire Valley Institute for Advanced Studies.

References:

(1) Burkholder, J. B.; Cox, R. A.; Ravishankara, A. R. Atmospheric Degradation of Ozone Depleting Substances, Their Substitutes, and Related Species. *Chem. Rev.* **2015**, *115* (10), 3704–3759.

(2) World Meteorological Organization; United States; National Oceanic and Atmospheric Administration; United States; National Aeronautics and Space Administration; United Nations Environment Programme; European Commission. *Scientific Assessment of Ozone Depletion: 2018, Highlights, ES.3, p. 47.*; **2019**.

(3) Hodnebrog, Ø.; Etminan, M.; Fuglestvedt, J. S.; Marston, G.; Myhre, G.; Nielsen, C. J.; Shine, K. P.; Wallington, T. J. Global Warming Potentials and Radiative Efficiencies of Halocarbons and Related Compounds: A Comprehensive Review. *Rev. Geophys.* **2013**, *51* (2), 300–378.

(4) Rust, D.; Katharopoulos, I.; Vollmer, M. K.; Henne, S.; O'Doherty, S.; Say, D.; Emmenegger, L.; Zenobi, R.; Reimann, S. Swiss Halocarbon Emissions for 2019 to 2020 Assessed from Regional Atmospheric Observations. *Atmospheric Chem. Phys.* **2022**, *22* (4), 2447–2466. https://doi.org/10.5194/acp-22-2447-2022.

(5) Mota-Babiloni, A.; Makhnatch, P. Predictions of European Refrigerants Place on the Market Following F-Gas Regulation Restrictions. *Int. J. Refrig.* **2021**, *127*, 101–110. https://doi.org/10.1016/j.ijrefrig.2021.03.005.

(6) Vereecken, L.; Aumont, B.; Barnes, I.; Bozzelli, J. W.; Goldman, M. J.; Green, W. H.; Madronich, S.; McGillen, M. R.; Mellouki, A.; Orlando, J. J. Perspective on Mechanism Development and Structure-Activity Relationships for Gas-Phase Atmospheric Chemistry. *Int. J. Chem. Kinet.* **2018**, *50* (6), 435–469.

(7) Lim, J. S. EPI Suite: A Fascinate Predictive Tool for Estimating the Fates of Organic Contaminants. *J. Bioremediat. Biodegrad.* **2016**, *7*, e171.

(8) US EPA, *EPI Suite™-Estimation Program Interface*. https://www.epa.gov/tsca-screening-tools/epi-suitetm-estimation-program-interface (accessed 2022-07-06).

(9) Kwok, E. S.; Atkinson, R. Estimation of Hydroxyl Radical Reaction Rate Constants for Gas-Phase Organic Compounds Using a Structure-Reactivity Relationship: An Update. *Atmos. Environ.* **1995**, *29* (14), 1685–1695.

(10) Atkinson, R. Kinetics and Mechanisms of the Gas-Phase Reactions of the Hydroxyl Radical with Organic Compounds under Atmospheric Conditions. *Chem. Rev.* **1986**, *86* (1), 69–201.

(11) Atkinson, R. A Structure-Activity Relationship for the Estimation of Rate Constants for the Gas-Phase Reactions of OH Radicals with Organic Compounds. *Int. J. Chem. Kinet.* **1987**, *19* (9), 799–828.

(12) Atkinson, R. Estimation of Gas-Phase Hydroxyl Radical Rate Constants for Organic Chemicals. *Environ. Toxicol. Chem. Int. J.* **1988**, *7* (6), 435–442.

(13) Tokuhashi, K.; Takizawa, K.; Kondo, S. Rate Constants for the Reactions of OH Radicals with $CF_3CX=CY_2$ (X= H, F, CF_3, Y= H, F, Cl). *Environ. Sci. Pollut. Res.* **2018**, *25* (15), 15204–15215.

(14) Tokuhashi, K.; Uchimaru, T.; Takizawa, K.; Kondo, S. Rate Constants for the Reactions of OH Radical with the (*E*)/(*Z*) Isomers of $CF_3CF{=}CHCl$ and $CHF_2CF{=}CHCl$. *J. Phys. Chem. A* **2018**, *122* (12), 3120–3127.

(15) Tokuhashi, K.; Takizawa, K.; Kondo, S. Rate Constants for the Reactions of OH Radicals with Fluorinated Ethenes: Kinetic Measurements and Correlation between Structure and Reactivity. *J. Phys. Chem. A* **2018**, *122* (19), 4593–4600.

(16) Tokuhashi, K.; Uchimaru, T.; Takizawa, K.; Kondo, S. Rate Constants for the Reactions of OH Radicals with the (*E*)/(*Z*) Isomers of CFCl=CFCl and (*E*)-CHF=CHF. *J. Phys. Chem. A* **2019**, *123* (23), 4834–4843.

(17) Tokuhashi, K.; Takizawa, K.; Kondo, S. Rate Constants for Reactions of OH Radicals with (*Z*)-$CF_3CCl=CHCl$, $CHF_2CF=CF_2$, (*E*)-$CF_3CH=CHF$, (*Z*)-$CF_3CH=CHF$, $CH_3CF=CH_2$, and $CH_2FCH=CH_2$. *Atmos. Environ.* **2021**, *255*, 118428.

(18) Orkin, V. L.; Huie, R. E.; Kurylo, M. J. Rate Constants for the Reactions of OH with HFC-245cb ($CH_3CF_2CF_3$) and Some Fluoroalkenes (CH_2CHCF_3, CH_2CFCF_3, CF_2CFCF_3, and CF_2CF_2). *J. Phys. Chem. A* **1997**, *101* (48), 9118–9124.

(19) Andersen, M. S.; Nielsen, O. J.; Toft, A.; Nakayama, T.; Matsumi, Y.; Waterland, R. L.; Buck, R. C.; Hurley, M. D.; Wallington, T. J. Atmospheric Chemistry of $C_xF_{2x+1}CHCH_2$ (x = 1, 2, 4, 6, and 8): Kinetics of Gas-Phase Reactions with Cl Atoms, OH Radicals, and O_3. *J. Photochem. Photobiol. Chem.* **2005**, *176* (1–3), 124–128.

(20) Nakayama, T.; Takahashi, K.; Matsumi, Y.; Toft, A.; Sulbaek Andersen, M. P.; Nielsen, O. J.; Waterland, R. L.; Buck, R. C.; Hurley, M. D.; Wallington, T. J. Atmospheric Chemistry of $CF_3CH=CH_2$ and $C_4F_9CH=CH_2$: Products of the Gas-Phase Reactions with Cl Atoms and OH Radicals. *J. Phys. Chem. A* **2007**, *111* (5), 909–915.

(21) Calvert, J. G.; Orlando, J. J.; Stockwell, W. R.; Wallington, T. J. *The Mechanisms of Reactions Influencing Atmospheric Ozone*; Oxford University Press, 2015.

(22) González, S.; Jiménez, E.; Ballesteros, B.; Martínez, E.; Albaladejo, J. Hydroxyl Radical Reaction Rate Coefficients as a Function of Temperature and IR Absorption Cross Sections for $CF_3CH{=}CH_2$ (HFO-1243zf), Potential Replacement of CF_3CH_2F (HFC-134a). *Environ. Sci. Pollut. Res.* **2015**, *22* (7), 4793–4805.

(23) Ballesteros, B.; Jiménez, E.; Moreno, A.; Soto, A.; Antiñolo, M.; Albaladejo, J. Atmospheric Fate of Hydrofluoroolefins, $C_xF_{2x+1}CHCH_2$ (x= 1, 2, 3, 4 and 6): Kinetics with Cl Atoms and Products. *Chemosphere* **2017**, *167*, 330–343.

(24) Atkinson, R.; Aschmann, S. M.; Carter, W. P. Effects of Ring Strain on Gas-Phase Rate Constants. 2. OH Radical Reactions with Cycloalkenes. *Int. J. Chem. Kinet.* **1983**, *15* (11), 1161–1177.

(25) Mellouki, A.; Teton, S.; Le Bras, G. Kinetics of OH Radical Reactions with a Series of Ethers. *Int. J. Chem. Kinet.* **1995**, *27* (8), 791–805.

(26) Othmani, H. E.; Ren, Y.; Mellouki, A.; Daële, V.; McGillen, M. R. Gas-Phase Rate Coefficient of OH + Cyclohexene Oxide Measured from 251 to 373 K. *Chem. Phys. Lett.* **2021**, *783*, 139056. https://doi.org/10.1016/j.cplett.2021.139056.

(27) Le Calvé, S.; Hitier, D.; Le Bras, G.; Mellouki, A. Kinetic Studies of OH Reactions with a Series of Ketones. *J. Phys. Chem. A* **1998**, *102* (24), 4579–4584.

(28) McGillen, M. R.; Carter, W. P.; Mellouki, A.; Orlando, J. J.; Picquet-Varrault, B.; Wallington, T. J. Database for the Kinetics of the Gas-Phase Atmospheric Reactions of Organic Compounds. *Earth Syst. Sci. Data* **2020**, *12* (2), 1203–1216.

(29) IUPAC: Task Group on Atmospheric Chemical Kinetic Data Evaluation, Task Group on Atmospheric Chemical Kinetic Data Evaluation, available at: http://iupac.pole-ether.fr/ (last access: 25 July 2022), **2019**.

(30) McGillen, M. R.; Percival, C. J.; Shallcross, D. E.; Harvey, J. N. Is Hydrogen Abstraction an Important Pathway in the Reaction of Alkenes with the OH Radical? *Phys. Chem. Chem. Phys.* **2007**, *9* (31), 4349–4356.

(31) Pinter, B.; Fievez, T.; Bickelhaupt, F. M.; Geerlings, P.; Proft, F. D. On the Origin of the Steric Effect. *Phys. Chem. Chem. Phys.* **2012**, *14* (28), 9846–9854. https://doi.org/10.1039/C2CP41090G.

(32) Hansch, C.; Leo, A.; Taft, R. W. A Survey of Hammett Substituent Constants and Resonance and Field Parameters. *Chem. Rev.* **1991**, *91* (2), 165–195.

(33) Brioude, J.; Portmann, R. W.; Daniel, J. S.; Cooper, O. R.; Frost, G. J.; Rosenlof, K. H.; Granier, C.; Ravishankara, A.; Montzka, S. A.; Stohl, A. Variations in Ozone Depletion Potentials of Very Short-Lived Substances with Season and Emission Region. *Geophys. Res. Lett.* **2010**, *37* (19).

(34) Wuebbles, D. J.; Patten, K. O.; Johnson, M. T.; Kotamarthi, R. New Methodology for Ozone Depletion Potentials of Short-Lived Compounds: N-Propyl Bromide as an Example. *J. Geophys. Res. Atmospheres* **2001**, *106* (D13), 14551–14571.

For TOC only

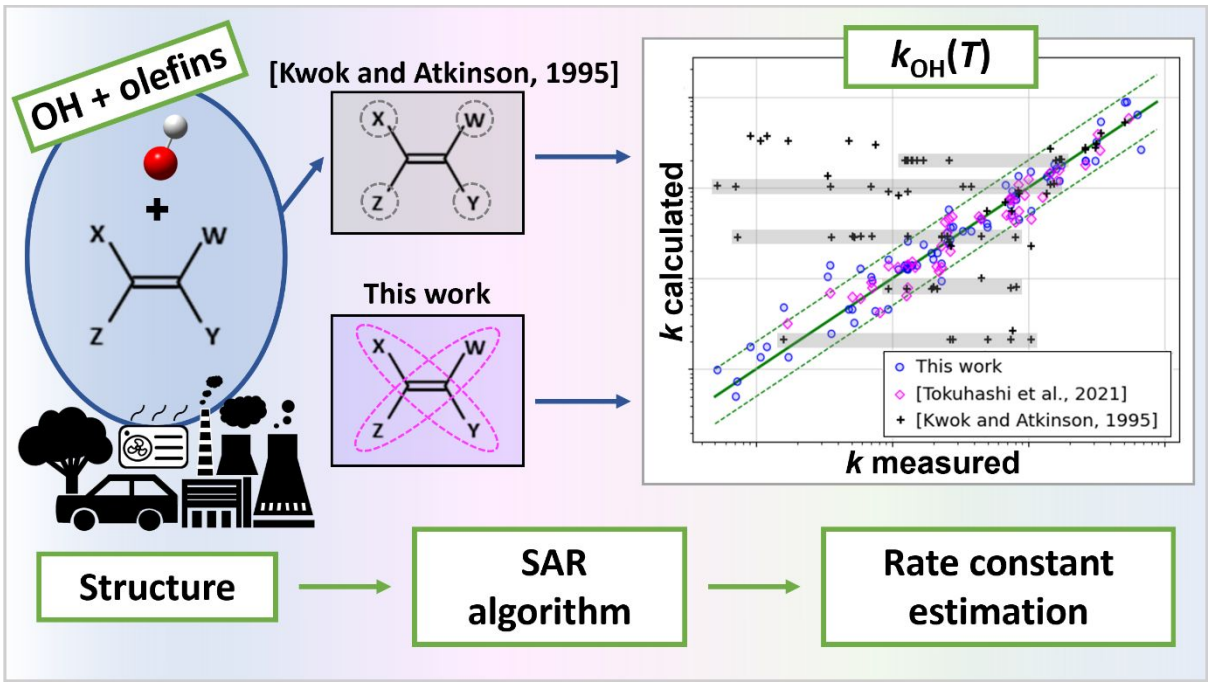
OH + olefins
[Kwok and Atkinson, 1995]
This work
X
W
Z
Y
$k_{OH}(T)$
k calculated
k measured
This work
[Tokuhashi et al., 2021]
[Kwok and Atkinson, 1995]
Structure
SAR algorithm
Rate constant estimation